Semibatch monomer addition as a general method to tune and enhance the mechanics of polymer networks via loop-defect control

Yuwei Gu[a], Ken Kawamoto[a], Mingjiang Zhong[a,b], Mao Chen[a], Michael J. A. Hore[c], Alex M. Jordan[c], LaShanda T. J. Korley[c], Bradley D. Olsen[b], and Jeremiah A. Johnson[a,1]

[a]Department of Chemistry, Massachusetts Institute of Technology, Cambridge, MA 02139; [b]Department of Chemical Engineering, Massachusetts Institute of Technology, Cambridge, MA 02139; and [c]Department of Macromolecular Science and Engineering, Case Western Reserve University, Cleveland, OH 44106

Edited by Steve Granick, IBS Center for Soft and Living Matter, Ulju-gun, Ulsan, Republic of Korea, and approved March 30, 2017 (received for review December 21, 2016)

Controlling the molecular structure of amorphous cross-linked polymeric materials is a longstanding challenge. Herein, we disclose a general strategy for precise tuning of loop defects in covalent polymer gel networks. This "loop control" is achieved through a simple semibatch monomer addition protocol that can be applied to a broad range of network-forming reactions. By controlling loop defects, we demonstrate that with the same set of material precursors it is possible to tune and in several cases substantially improve network connectivity and mechanical properties (e.g., ∼600% increase in shear storage modulus). We believe that the concept of loop control via continuous reagent addition could find broad application in the synthesis of academically and industrially important cross-linked polymeric materials, such as resins and gels.

gels | loops | polymer networks | click chemistry | star polymer

Polymer networks are extensively used in fields where elastic yet tough materials with relatively low moduli are needed, such as tissue engineering (1, 2), optical actuation (3), soft electronics (4), and autonomous materials (5, 6). The bulk properties of polymer networks are highly sensitive to the presence of defects, such as loops, that can be difficult to quantify and control (7–12). Here, we report that semibatch monomer addition provides a universal method to precisely control the number of loop defects in constitutionally isomeric polymer networks. This method yields materials with improved connectivity and enhanced mechanical properties compared with their batch-synthesized counterparts. We quantitatively prove the reduction of loops afforded by semibatch addition through a technique called star network disassembly spectrometry.

We focused our efforts on end-linked star polymer gels (13–18), which are a broadly useful class of polymer networks (Fig. 1). In an end-linked polymer gel prepared from a bifunctional monomer (A_2) and a star polymer with f arms (B_f), the simplest cyclic defects (7, 19, 20), primary (1°) loops, have the greatest impact on bulk mechanical properties (12) (Fig. 1). Although we have reported several methods for counting 1° loops in polymer networks (21–23), none can currently be applied to star polymer networks.

In polymer network synthesis, the network components ("monomers") are typically mixed together at the same time and allowed to undergo a cross-linking reaction. In such cases, the network topology is set by the monomer composition and the network concentration. We realized that the rate of addition of B_f to A_2 could provide a way to modify network topology in networks made from the same components and formed at the same concentration (Fig. 2). This concept is rationalized schematically in Fig. 2*A* for an $A_2 + B_4$ network-forming reaction where the B_4 component is added slowly to a solution of A_2. In such a system, because A_2 is present in large excess, the chain ends of network fragments produced before the gel point are capped with dangling "A" groups that cannot form a 1° loop. If slow addition of B_4 was carried out to near the gel point, and a final bolus addition of B_4 was then added to reach 1:1 A:B stoichiometry, then the resulting material would have fewer loops compared to the batch-synthesized network formed at the same concentration.

Semibatch reagent addition is a ubiquitous tactic in synthetic organic chemistry; it is easily achieved on laboratory scale using a conventional syringe pump apparatus (Fig. 2*B*). Although semibatch processes have been exploited in small-molecule synthesis (24, 25) and polymerization (26–32), and analogous continuous flow processes have enabled transformations in organic and polymer chemistry (33–35), these methods have not, to our knowledge, been used to control the topology and bulk mechanical properties of polymer networks.

Counting 1° Loops in Star Polymer Networks

We first sought to examine the effect of monomer feed rate on the fraction of 1° loops in star polymer networks. We developed the star network disassembly spectrometry method as outlined in Fig. 3*A* for a gel prepared from bis-cyclooctyne $\mathbf{A_2}$ and tetra-azide PEG star polymers $\mathbf{B_{4H}}$ and $\mathbf{B_{4D}}$ (10-kDa number-average molar mass, M_n; *SI Appendix*, sections SII and SVI). Mixing of these components leads to network formation via strain-promoted azide–alkyne cycloaddition (SPAAC) (36–39). The star polymers $\mathbf{B_{4H}}$ and $\mathbf{B_{4D}}$ possess photocleavable *ortho*-nitrobenzyloxycarbonyl (NBOC) groups (40, 41) near their termini that facilitate controlled network disassembly in response to UV light (358 nm). They also possess either hydrogen ($\mathbf{B_{4H}}$) or deuterium ($\mathbf{B_{4D}}$) labels between the azide and the NBOC groups. Consequently, network formation and disassembly leads to three possible labeled products: **nn**, **ni**, and **ii** (Fig. 3*A*). The ratios of these products (Fig. 3*B*) are uniquely dependent on the fraction of 1° loops per doubly reacted $\mathbf{A_2}$, denoted here as ϕ_λ, and the amount of $\mathbf{B_{4H}}$ and $\mathbf{B_{4D}}$ used to form the network (x and $1 - x$, respectively) according to Eqs. **1** and **2** (*SI Appendix*, section SIII.A)

Significance

We demonstrate that slow monomer addition during step-growth polymer network formation changes the fraction of loop defects within the network, thus providing materials with tunable and significantly improved mechanical properties. This phenomenon is general to a range of network-forming reactions and offers a powerful method for tuning the mechanics of materials without changing their composition.

Author contributions: Y.G., K.K., M.Z., M.C., B.D.O., and J.A.J. designed research; Y.G., K.K., M.Z., M.C., M.J.A.H., and A.M.J. performed research; Y.G., M.J.A.H., A.M.J., and L.T.J.K. contributed new reagents/analytic tools; Y.G., K.K., M.Z., M.C., M.J.A.H., A.M.J., L.T.J.K., B.D.O., and J.A.J. analyzed data; and Y.G. and J.A.J. wrote the paper.

The authors declare no conflict of interest.

This article is a PNAS Direct Submission.

[1]To whom correspondence should be addressed. Email: jaj2109@mit.edu.

This article contains supporting information online at www.pnas.org/lookup/suppl/doi:10.1073/pnas.1620985114/-/DCSupplemental.

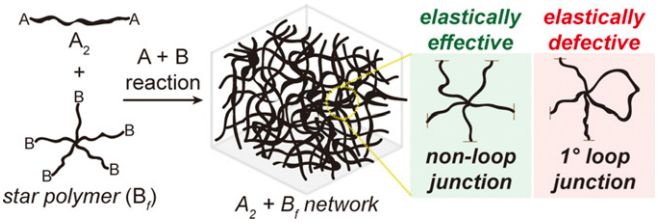

Fig. 1. End-linked polymer networks/gels are prepared by coupling of multifunctional molecules, e.g., $A_2 + B_f$. The properties of such networks are defined by their connectivity, branch functionality, and topology. Cyclic defects, such as the 1° loop, are elastically defective.

$$\frac{[nn]}{[ii]} = \frac{x^2(1-\phi_\lambda) + x\phi_\lambda}{(1-x)^2(1-\phi_\lambda) + (1-x)\phi_\lambda}, \quad [1]$$

$$\frac{[ni]}{[ii]} = \frac{2x(1-x)(1-\phi_\lambda)}{(1-x)^2(1-\phi_\lambda) + (1-x)\phi_\lambda}. \quad [2]$$

Notably, because star network disassembly spectrometry yields three disassembly products (**nn**, **ni**, and **ii**) regardless of f, this strategy should be universal to a range of f-functional star polymers with no additional complications from higher f junctions: a significant advance over our previous loop-counting methods.

We validated star network disassembly spectrometry using gels formed at various network concentrations. DMSO stock solutions of $\mathbf{A_2}$ and 1 $\mathbf{B_{4H}}$:1 $\mathbf{B_{4D}}$ (i.e., $x = 0.5$) and additional DMSO were mixed to achieve the desired concentration and a 1:1 ratio of functional groups A (cyclooctyne) and B (azide). The reactions were allowed to proceed under ambient atmosphere for 24 h to achieve maximal conversion (>98%; *SI Appendix*, section SIII.B). Then, the gels were exposed to UV irradiation (358-nm, 8-W bench-top lamp) for 5 h to generate the mixture of disassembly products shown in Fig. 3*A*. The distribution of **nn**, **ni**, and **ii** was obtained by electrospray ionization mass spectrometry (see Fig. 3*B* for example spectrum). Application of Eqs. **1** and **2** provided ϕ_λ as a function of network concentration (Fig. 3*C*). As expected, ϕ_λ decreased as polymer concentration increased, which reflects the intramolecular nature of 1° loop formation. A sol–gel transition occurred at ∼1.5 mM (1.5% m/v); below this concentration gelation was precluded by the large number of loops. The experimental results were compared with rate theory methods developed by us (23) (*SI Appendix*, section SIII.G). The experiment and theory are in excellent agreement. Taken together, these results show that star network disassembly spectrometry can be used to precisely and accurately count loops in star polymer networks.

Monomer Feed Rate and Network Topology

We next studied the impact of monomer addition rate on ϕ_λ in these materials. For these studies, 20 μL of a 40 mM $\mathbf{A_2}$ solution was placed in a vial, to which 380 μL of 1.05 mM $\mathbf{B_4}$ solution was added (1 μL/min) over 6.3 h via a digitally programmable syringe pump to reach 1:1 stoichiometry of functional groups and 1 mM (1% m/v) final concentration of $\mathbf{B_4}$ (note: "$\mathbf{B_4}$" refers to a 1:1 mixture of $\mathbf{B_{4H}}$ and $\mathbf{B_{4D}}$). The reaction was monitored over time to determine ϕ_λ as a function of the percentage of $\mathbf{B_4}$ added (Fig. 4*A*).

During the course of slow $\mathbf{B_4}$ addition, ϕ_λ gradually decreased. Upon completion, a polymer network with $\phi_\lambda = 19\%$ was obtained (Fig. 4*A*). Note that in Fig. 4*A*, at early stages of the network-forming reaction ϕ_λ is quite large. This observation highlights the fact that ϕ_λ is the fraction of loops on doubly reacted $\mathbf{A_2}$. At early stages, there is very little doubly reacted $\mathbf{A_2}$ (most $\mathbf{A_2}$ molecules are either unreacted or reacted on only one end); what little does exist is likely to be a 1° loop. Importantly, at complete conversion the analogous batch-prepared material had $\phi_\lambda = 35\%$. Thus, slow addition afforded a material with nearly 50% fewer 1° loops. Rate theory calculations of ϕ_λ supported these experimental findings (Fig. 4*A*). This reduction in defects was reflected as a change in the material properties: slow addition produced elastic gels (solids) (Fig. 4*B*) whereas the batch process gave a fluid.

Next, we prepared a series of networks using different rates of B_4 addition (u). As shown in Fig. 4*B*, ϕ_λ decreases as u decreases until u approaches 2 μL/min, where ϕ_λ reaches a constant value. We developed a semiquantitative model to interpret the data (*SI Appendix*, section SIV.C). Given the reported second-order rate constant of this SPAAC reaction (0.3 $M^{-1}{\cdot}s^{-1}$) (42), the model predicts that for $u \leq 2.75$ μL/min there should be no further reduction in loop defects. The agreement between the predicted and observed data (Fig. 4*B*) supports our proposed mechanism (Fig. 2*A*). To provide further evidence, we used liquid chromatography and UV absorbance to quantify the fraction of dangling cyclooctynes as a function of the percentage of $\mathbf{B_4}$ added via slow addition (*SI Appendix*, Fig. S4). As expected, the fraction of dangling A groups was very high at early stages in the reaction (due to a large excess of $\mathbf{A_2}$ monomer) and it gradually decreased to undetectable

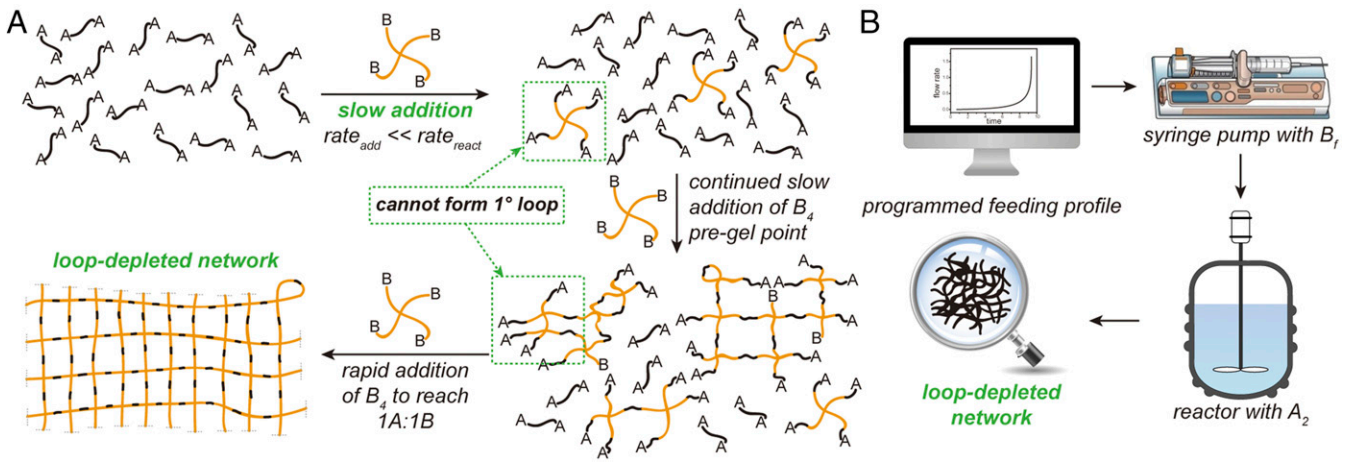

Fig. 2. Rationale and process for loop control via programmed monomer addition. (*A*) Schematic for network formation via slow then fast addition of B_4 to a solution of A_2. (*B*) Programmed semibatch network synthesis using a syringe pump leads to loop-depleted networks.

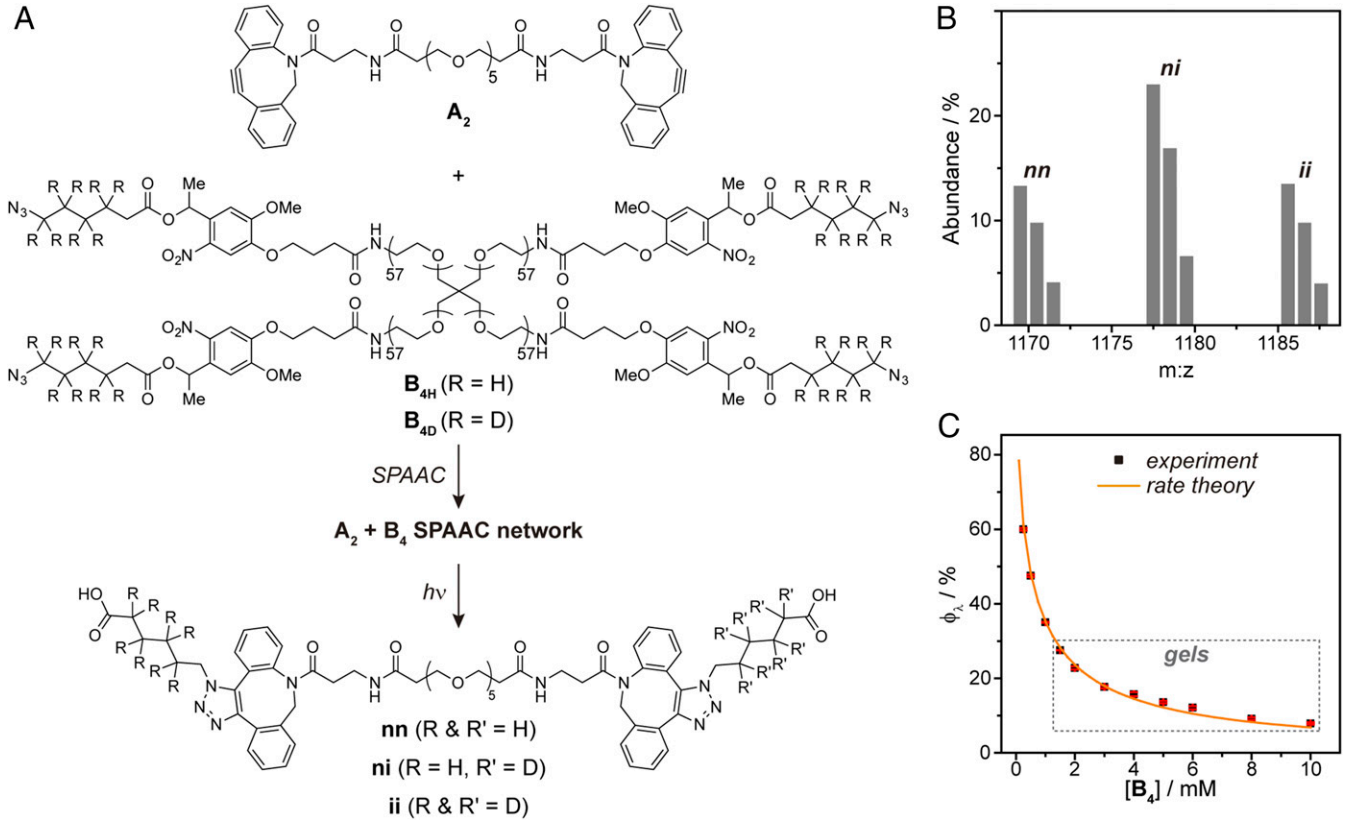

Fig. 3. Star network disassembly spectrometry. (*A*) Chemical structures of compounds $\mathbf{A_2}$, $\mathbf{B_{4H}}$, and $\mathbf{B_{4D}}$. Combining $\mathbf{A_2}$ with a 1:1 mixture of $\mathbf{B_{4H}}$ and $\mathbf{B_{4D}}$ leads to $A_2 + B_4$ networks via SPAAC. Exposure of these materials to UV light induces network disassembly to yield three labeled products: **nn**, **ni**, and **ii**. (*B*) A representative mass spectrum showing the products **nn**, **ni**, and **ii**. The ratios of these products are uniquely dependent on ϕ_λ. (*C*) Plot of ϕ_λ versus $[\mathbf{B_4}]$ as obtained by experiments and rate theory. m, mass; z, charge.

levels as the addition proceeded. These dangling ends suppress loop formation and lead to loop-depleted networks (Fig. 2*A*).

Given that slow addition has the greatest impact on ϕ_λ during the earliest stages of network formation, we also investigated a "slow then fast" (STF) addition approach wherein the first 50% of $\mathbf{B_4}$ solution was added slowly to yield soluble "A-rich" network fragments (Fig. 2*A*) and the second 50% was added in one portion to induce gelation. As shown in Fig. 4*A*, the STF method gave $\phi_\lambda = 21\%$, which is similar to the result obtained for complete slow addition (19%). Notably, STF addition provides a faster and more convenient way to reduce the number of loop defects that avoids concerns over gelation before complete monomer addition.

Having demonstrated both slow addition and STF addition methods as promising for tuning the number of loops at a concentration that does not produce gels upon batch mixing (1 mM, 1% m/v), we investigated whether the same methods could enable the synthesis of loop-depleted polymer networks at concentrations much higher than the gel point for the batch-synthesized material. Gels were prepared via slow addition and STF addition as described above but with concentrations adjusted to yield a final $[\mathbf{B_4}]$ of 5 mM (5% m/v) (note: this concentration is half that of the solubility limit of the $\mathbf{B_4}$ star polymer; see *SI Appendix*). In the case of complete slow addition, the gel point was reached long before $\mathbf{B_4}$ could be completely added, which led to a large amount of undesirable sol fraction. Thus, we focused on the STF method. As shown in Table 1, STF addition once again yielded networks with nearly 50% fewer 1° loops compared with batch synthesis.

We used Fourier transform infrared spectroscopy (FTIR), swelling measurements, and small-angle neutron scattering (SANS) to characterize gels prepared via STF and batch methods. The FTIR spectra (*SI Appendix*, Fig. S7) for these materials were indistinguishable, which suggests that STF does not lead to a significant change in the chemical composition of the network. The swelling ratio S, which is the ratio of the solvent-swollen gel divided by the dried gel, for the STF-formed material was significantly lower than that of the material formed via batch mixing (Table 1), which supports the notion that the STF-formed material has fewer topological defects. The SANS curves (Fig. 4*C*) were fitted using the following model, which combines a power law with an Ornstein–Zernike function (43):

$$I(q) = \frac{A}{q^n} + \frac{C}{1 + (q\xi_L)^m} + B,$$

where q is the scattering vector, ξ_L is the network mesh size, n is a scaling exponent for scattering from the larger network structure, m is a scaling exponent for scattering from polymer chains, A and C are constants, and B the incoherent background. STF addition reduced ξ_L by ~0.6 nm (Table 1). Given that the concentration of $\mathbf{B_4}$ is below the overlap concentration of the 10-kDa four-arm PEG star polymer ($\phi^* = 6$ mM, 6% m/v) and that the A and B functional groups are present in equal stoichiometry, the observation of a decreased mesh size ξ_L is consistent with increased network homogeneity at short length scales, which is expected for a reduction in the fraction of 1° loops (44). We also note that STF addition leads to an increase in low-q scattering, which suggests that there may be some increase in long length-scale heterogeneities within the gel (45).

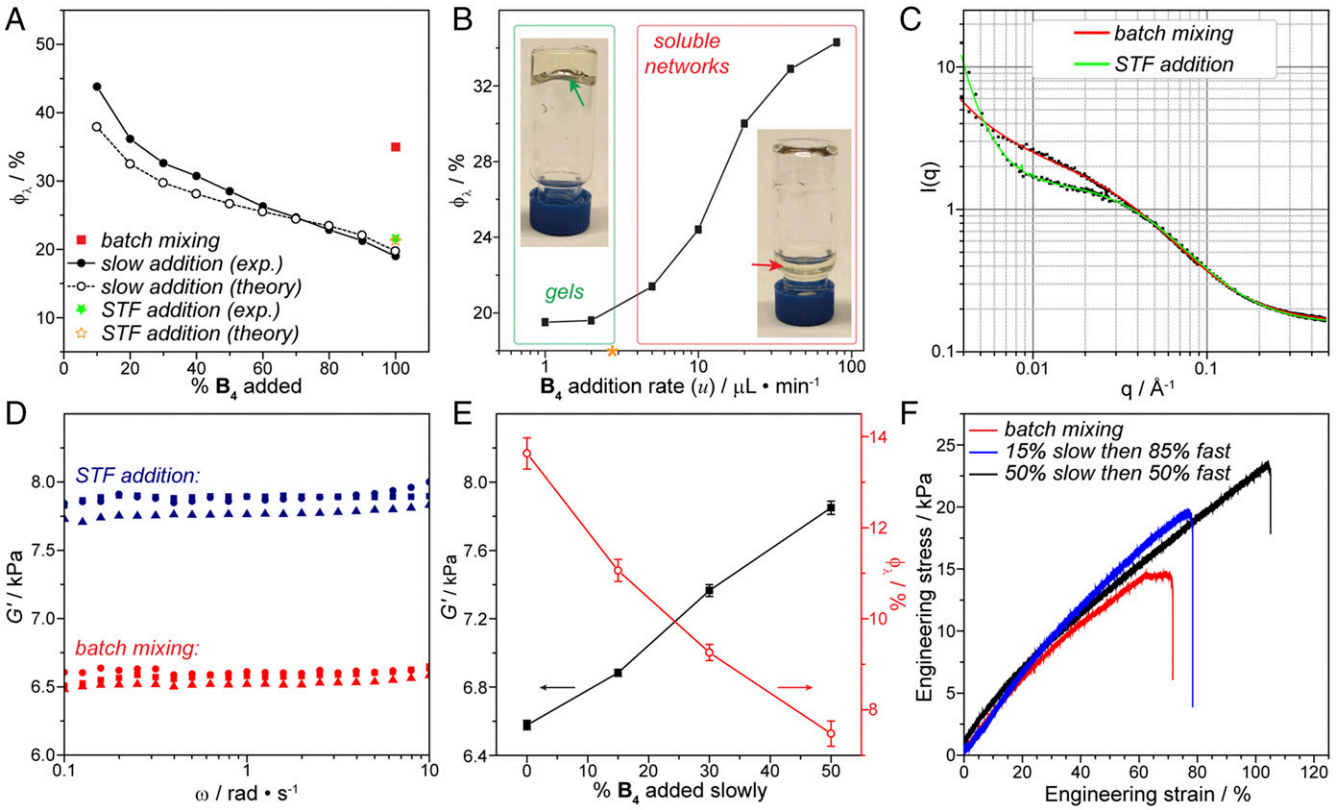

Fig. 4. Controlled monomer addition leads to reduction of loop defects in PEG gels prepared via SPAAC. (*A*) ϕ_λ as a function of batch mixing, slow addition, and STF addition of $\mathbf{B_4}$ to $\mathbf{A_2}$ (final concentration of $\mathbf{B_4}$ is 1 mM for all samples). Slow addition and STF addition both provide a significant decrease in ϕ_λ. Rate theory calculations (open circles) follow a similar trend. (*B*) Effect of $\mathbf{B_4}$ addition rate (u) on ϕ_λ. * denotes the predicted addition rate $u = 2.75$ μL/min below which ϕ_λ should not change significantly. This prediction is based on the reported second-order rate constant for DBCO and azide SPAAC (0.3 $M^{-1}{\cdot}s^{-1}$). (*C*) SANS curves for gels prepared at $\mathbf{B_4}$ = 5 mM using batch addition and STF addition. (*D*) Plots of G' versus frequency for gels prepared at $\mathbf{B_4}$ = 5 mM using batch addition versus STF addition. (*E*) Relationships between G', ϕ_λ, and the percentage of $\mathbf{B_4}$ added slowly. (*F*) Representative tensile testing measurements of gels prepared at $\mathbf{B_4}$ = 5 mM using batch addition and STF addition with 15% versus 50% of $\mathbf{B_4}$ added slowly.

Using STF Addition to Improve and Tune Gel Mechanics

Next, we studied how the structural changes imparted by STF addition impact the bulk mechanical properties of these gels. Fig. 4*D* shows plots of the shear storage modulus G' versus frequency for gels prepared at $[\mathbf{B_4}] = 5$ mM (5% m/v) by batch monomer mixing and STF addition (note: three gels of each type were prepared and G'' was omitted for clarity; *SI Appendix*, Fig. S8). Whereas both methods yielded elastic materials (as demonstrated by rheology and creep and recovery tests shown in *SI Appendix*, Fig. S12), the gels formed via STF addition consistently possessed ~19% greater G' values despite the fact that they were formed at exactly the same concentration and using the same components as the batch-formed gels (Table 1). This mechanical enhancement is due to the reduction in loop defects afforded by STF addition. Moreover, we note that STF addition gave similar improvements in G' for gels formed above and below the overlap concentration (*SI Appendix*, Figs. S11 and S13). We can estimate the impact of 1° loops on G' via the real elastic network theory (12):

$$G = G_0\left(1 - \frac{8}{3}\phi_\lambda\right),$$

where G_0 is the modulus of an ideal network with no defects and G is the modulus of the real network. The measured ϕ_λ and G' values correlated well (*SI Appendix*, Table S9), which further highlights the impact of 1° loops on the storage modulus. Moreover, tensile tests showed that STF addition yielded materials with greater tensile moduli relative to batch addition (Fig. 4*F* and *SI Appendix*, Fig. S10).

As shown in Fig. 4*E*, as the percentage of $\mathbf{B_4}$ monomer that was added slowly was gradually increased, ϕ_λ decreased and G' increased. Thus, through simply altering the amount of $\mathbf{B_4}$ monomer added slowly, it was possible to finely tune the loop content of these networks, and thereby produce a series of gels of the same composition and concentration with an ~19% variation in G'. Depending on the network structure and composition, the extent of this range will of course vary; nonetheless, alterations, and particularly enhancements, of even a few percent in modulus could be valuable in specific applications given the simplicity of STF addition and the fact that new network components are not needed.

To investigate the effect of the order of addition on gel properties, we prepared a series of gels by slowly adding a solution of $\mathbf{A_2}$ to a solution of $\mathbf{B_4}$ (the opposite order as studied above). Interestingly, although star network disassembly spectrometry showed that ϕ_λ was indeed reduced via this method, there was no enhancement of the mechanical properties of the gels compared with the batch-mixing case (*SI Appendix*, section SV). These observations

Table 1. Characterization of PEG gels prepared via SPAAC and different addition methods ($[\mathbf{B_4}]$ = 5 mM, 5% m/v)

Sample	ϕ_λ, %	S	ξ_L, nm	G', Pa
Batch mixing	13.63 ± 0.34	41.2 ± 1.2	2.83 ± 0.05	6,578 ± 27
STF addition	7.48 ± 0.28	35.9 ± 0.7	2.23 ± 0.03	7,850 ± 39

suggest that inversing the order of addition leads to new defects [e.g., clusters of variable network density (46, 47) or higher order loops (12, 48)] that cancel the effect of reducing ϕ_λ. SANS analysis is consistent with this hypothesis: the mesh size for this gel was larger (4.32 ± 0.05 nm; *SI Appendix*, Table S11) than that for the batch-addition sample (2.83 ± 0.05 nm) despite its lower fraction of 1° loops.

Generality of STF Addition

We tested STF addition in other network-forming systems to demonstrate that the property enhancements observed above are general even in materials where we cannot directly count loops. First, another $A_2 + B_4$ network was prepared via thiol-maleimide conjugate addition of commercially available PEG components. In this hydrogel system, STF addition led to gelation at a concentration well below the gel point of batch-synthesized gels (*SI Appendix*, Fig. S18). Moreover, a doubling of G' was achieved for gels prepared at 4.5 mM via STF versus batch (*SI Appendix*, Fig. S19).

Next, a network derived from 10-kDa eight-arm PEG amine ($\mathbf{B_{8NH2}}$) and suberic acid bis(*N*-hydroxysuccinimidyl ester) ($\mathbf{A_{2NHS}}$) was investigated (Fig. 5*A*). In this system, the sol–gel point occurs at $[\mathbf{B_{8NH2}}]$ = 2.25 mM (2.25% m/v) when both components are mixed in batch. Fig. 5*B* shows that when a solution of $\mathbf{B_{8NH2}}$ was added slowly to a solution of $\mathbf{A_{2NHS}}$, gels formed at concentrations as low as $[\mathbf{B_{8NH2}}]$ = 1.5 mM (1.5% m/v). Moreover, G' values for gels formed via STF addition ($[\mathbf{B_{8NH2}}]$ = 2.5 mM, 2.5% m/v) were nearly six times greater than those formed via batch addition (1,300 Pa compared with 220 Pa, respectively) (Fig. 5*C*). We also note that when the gelation was performed above overlap concentration, a similar improvement in G' was still observed (*SI Appendix*, Fig. S16). To further prove that STF addition leads to tunable mechanical properties in these $f = 8$ networks, we prepared 4 different sets of $\mathbf{A_{2NHS}} + \mathbf{B_{8NH2}}$ gels at the same concentration ($[\mathbf{B_{8NH2}}]$ = 5 mM (5% m/v) but with different amounts of $\mathbf{B_{8NH2}}$ monomer added via the STF method (*SI Appendix*, Fig. S17). Similar to the studies described above, swelling ratio measurements and shear rheometry demonstrated that STF addition could produce gels at constant concentration with variable mechanical properties. Notably, compared with the $A_2 + B_4$ gels prepared by SPAAC, the range of storage moduli accessible in $\mathbf{A_{2NHS}} + \mathbf{B_{8NH2}}$ networks (from 9 to 15 kPa) is much larger, which suggests that STF addition may have a larger impact on high-f materials (49).

Pendantly functionalized polymers are frequently used as precursors to polymer networks, and we hypothesized that our loop-control strategy would also be applicable to these materials as they are analogous to end-linked networks where the B_f monomer has a distribution of f values. Thus, we synthesized pendantly azido-functionalized random copolymer with a number average of 24 azide groups ($\mathbf{B_{\sim 24}}$) using nitroxide mediated polymerization (Fig. 5*D*). Polymer networks were formed via SPAAC using this pendantly functionalized polymer and $\mathbf{A_2}$ (Fig. 5*D*). Fig. 5 *E* and *F* shows that STF addition has a similar impact on these pendantly

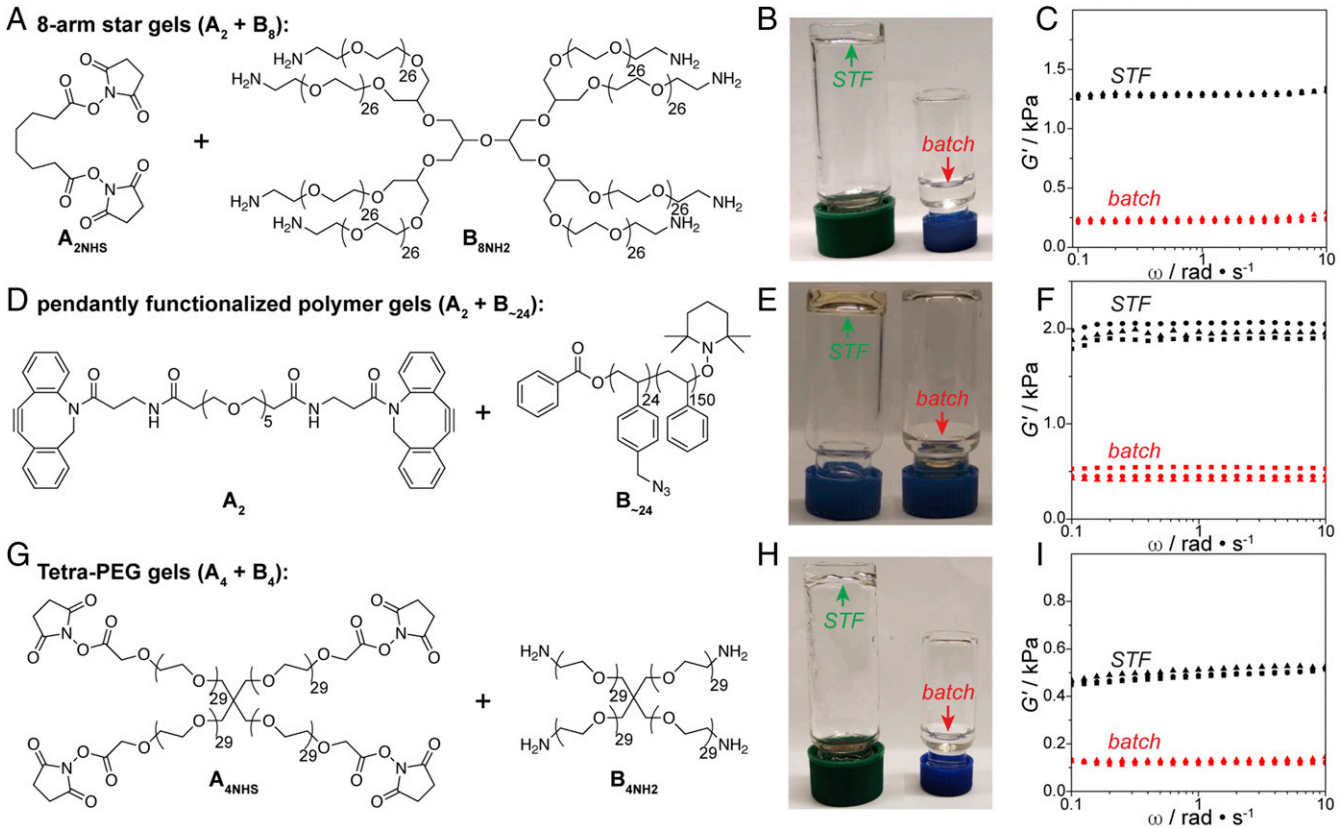

Fig. 5. Generality of loop control via STF addition. (*A*) Chemical structures of $A_2 + B_8$ network components. (*B*) STF addition of $\mathbf{A_{2NHS}}$ to $\mathbf{B_{8NH2}}$ at 1.5 mM leads to gelation (*Left*), whereas batch addition at the same concentration does not produce a gel (*Right*). (*C*) Shear moduli for $\mathbf{A_2} + \mathbf{B_8}$ gels formed via STF addition and batch addition at $\mathbf{B_{8NH2}}$ = 2.5 mM. STF addition leads to an ∼sixfold enhancement in G'. (*D*) Chemical structures of $\mathbf{A_2} + \mathbf{B_{\sim 24}}$ ($\mathbf{B_{\sim 24}}$ is a statistical copolymer) network components. (*E*) STF addition of $\mathbf{A_2}$ to $\mathbf{B_{\sim 24}}$ at 1.6 mM leads to gelation (*Left*), whereas batch addition at the same concentration does not produce a gel (*Right*). (*F*) Shear moduli for $\mathbf{A_2} + \mathbf{B_{\sim 24}}$ gels formed via STF addition and batch addition at $[\mathbf{B_{\sim 24}}]$ = 2 mM. STF addition leads to an ∼fourfold enhancement in G'. (*G*) Chemical structures of $A_4 + B_4$ Tetra-PEG network components. (*H*) STF addition of $\mathbf{A_{4NHS}}$ to $\mathbf{B_{4NH2}}$ at 1 mM leads to gelation (*Left*), whereas batch addition at the same concentration does not produce a gel (*Right*). (*I*) Shear moduli for Tetra-PEG gels formed via STF addition and batch addition at $\mathbf{B_{4NHS}}$ = 1.5 mM. rad, radians.

functionalized polymer networks, enabling an ~400% increase in G' for gels formed at $[\mathbf{B}_{\sim 24}] = 2$ mM.

Finally, we examined STF addition in the context of an $A_4 + B_4$ star polymer end-linking reaction that cannot form 1° loops. Although these "Tetra-PEG" gels inherently have highly homogeneous network structures and excellent mechanical properties (50) (Fig. 5*D*), they still have cyclic defects such as secondary loops (51). We have previously shown that the number of 1° loops is coupled to the numbers of higher order loops (48), and that these higher order defects are also elastically defective (12). We suspected that STF addition may reduce higher order loop defects in Tetra-PEG gels (45). This notion is supported by the results presented in Fig. 5*E*. Whereas STF addition of Tetra-PEG components $\mathbf{A_{4NHS}}$ and $\mathbf{B_{4NHS}}$ at 1 mM (1% m/v) led to gelation, batch addition at this same concentration did not produce gels (Fig. 5*E*). Rheological analysis for Tetra-PEG gels formed at 1.5 mM (1.5% m/v) showed a >300% increase in G' for STF addition compared with batch addition (Fig. 5*F*). When Tetra-PEG gels were prepared at higher concentration (5 mM) there was no discernible difference between batch addition and STF addition (*SI Appendix*, Fig. S21), which highlights the fact that higher order cyclic defects are not as detrimental to elasticity as 1° loops (12). Nonetheless, these data provide evidence that simple STF addition can reduce not only 1° loops but also higher order defects in polymer networks.

In summary, we have demonstrated semibatch monomer addition as a method for controlling the fraction of loops in polymer networks. The mechanism for this process was supported by an experimental method, star network disassembly spectrometry, that enables quantification of 1° loops in networks formed via end-linking of star polymers. STF addition is general to a range of network-forming systems, and it facilitates the synthesis of materials with enhanced and finely tuned mechanical properties. STF addition can even enable gelation below "normal" sol–gel transition points. These findings should prove useful for researchers interested in polymer networks in a range of industrial and academic settings.

Methods and Materials

Details of all procedures can be found in the *SI Appendix*. In general, monomer B_4 was dissolved in a desired amount of solvent and added slowly via a syringe pump to a solution of A_2 in the same solvent until the desired conversion was reached. Then, the remaining B_4 monomer was quickly added to achieve 1:1 functional group stoichiometry and the chosen final concentration.

ACKNOWLEDGMENTS. We thank S. L. Buchwald for the syringe pump and W. Zhang for help with FTIR measurements. We thank the National Science Foundation (CHE-1334703) for support of this work. We acknowledge the support of the National Institute of Standards and Technology, US Department of Commerce, in providing the neutron research facilities used in this work. This work made use of the Shared Experimental Facilities supported in part by the Materials Research Science and Engineering Centers Program of the National Science Foundation under Award DMR-1319807.

1. Lee KY, Mooney DJ (2001) Hydrogels for tissue engineering. *Chem Rev* 101:1869–1879.
2. Rosales AM, Anseth KS (2016) The design of reversible hydrogels to capture extracellular matrix dynamics. *Nat Rev Mater* 1:1–15.
3. Dong L, Agarwal AK, Beebe DJ, Jiang H (2006) Adaptive liquid microlenses activated by stimuli-responsive hydrogels. *Nature* 442:551–554.
4. Keplinger C, et al. (2013) Stretchable, transparent, ionic conductors. *Science* 341:984–987.
5. Li C-H, et al. (2016) A highly stretchable autonomous self-healing elastomer. *Nat Chem* 8:618–624.
6. He X, et al. (2012) Synthetic homeostatic materials with chemo-mechano-chemical self-regulation. *Nature* 487:214–218.
7. Wilcock DF (1947) Liquid methylpolysiloxane systems. *J Am Chem Soc* 69:477–486.
8. Flory PJ (1953) *Principles of Polymer Chemistry* (Cornell Univ Press, Ithaca, NY), p 349.
9. Rubinstein M, Colby RH (2003) *Polymer Physics* (Oxford Univ Press, Oxford), p 263.
10. Zhukhovitskiy AV, et al. (2016) Highly branched and loop-rich gels via formation of metal-organic cages linked by polymers. *Nat Chem* 8:33–41.
11. Müllen K (2016) Molecular defects in organic materials. *Nat Rev Mater* 1:15013.
12. Zhong M, Wang R, Kawamoto K, Olsen BD, Johnson JA (2016) Quantifying the impact of molecular defects on polymer network elasticity. *Science* 353:1264–1268.
13. Chen X, et al. (2002) A thermally re-mendable cross-linked polymeric material. *Science* 295:1698–1702.
14. Kloxin AM, Kasko AM, Salinas CN, Anseth KS (2009) Photodegradable hydrogels for dynamic tuning of physical and chemical properties. *Science* 324:59–63.
15. DeForest CA, Tirrell DA (2015) A photoreversible protein-patterning approach for guiding stem cell fate in three-dimensional gels. *Nat Mater* 14:523–531.
16. Kamata H, Akagi Y, Kayasuga-Kariya Y, Chung UI, Sakai T (2014) "Nonswellable" hydrogel without mechanical hysteresis. *Science* 343:873–875.
17. Xia Y, Verduzco R, Grubbs RH, Kornfield JA (2008) Well-defined liquid crystal gels from telechelic polymers. *J Am Chem Soc* 130:1735–1740.
18. Johnson JA, et al. (2006) Synthesis of degradable model networks via ATRP and click chemistry. *J Am Chem Soc* 128:6564–6565.
19. Rankin SE, Kasehagen LJ, McCormick AV, Macosko CW (2000) Dynamic Monte Carlo simulation of gelation with extensive cyclization. *Macromolecules* 33:7639–7648.
20. Lang M, Göritz D, Kreitmeier S (2005) Intramolecular reactions in randomly end-linked polymer networks and linear (co)polymerizations. *Macromolecules* 38:2515–2523.
21. Zhou H, et al. (2012) Counting primary loops in polymer gels. *Proc Natl Acad Sci USA* 109:19119–19124.
22. Zhou H, et al. (2014) Crossover experiments applied to network formation reactions: Improved strategies for counting elastically inactive molecular defects in PEG gels and hyperbranched polymers. *J Am Chem Soc* 136:9464–9470.
23. Kawamoto K, Zhong M, Wang R, Olsen BD, Johnson JA (2015) Loops versus branch functionality in model click hydrogels. *Macromolecules* 48:8980–8988.
24. Battilocchio C, et al. (2016) Iterative reactions of transient boronic acids enable sequential C-C bond formation. *Nat Chem* 8:360–367.
25. Kim H, et al. (2016) Submillisecond organic synthesis: Outpacing Fries rearrangement through microfluidic rapid mixing. *Science* 352:691–694.
26. Chen H, Kong J (2016) Hyperbranched polymers from A2+ B3 strategy: Recent advances in description and control of fine topology. *Polym Chem* 7:3643–3663.
27. Lin Q, Long TE (2003) Polymerization of A2 with B3 monomers: A facile approach to hyperbranched poly(aryl ester)s. *Macromolecules* 36:9809–9816.
28. Bharathi P, Moore JS (2000) Controlled synthesis of hyperbranched polymers by slow monomer addition to a core. *Macromolecules* 33:3212–3218.
29. Sunder A, Hanselmann R, Frey H, Mülhaupt R (1999) Controlled synthesis of hyperbranched polyglycerols by ring-opening multibranching polymerization. *Macromolecules* 32:4240–4246.
30. Harth E, et al. (2002) A facile approach to architecturally defined nanoparticles via intramolecular chain collapse. *J Am Chem Soc* 124:8653–8660.
31. Matyjaszewski K, Ziegler MJ, Arehart SV, Greszta D, Pakula T (2000) Gradient copolymers by atom transfer radical copolymerization. *J Phys Org Chem* 13:775–786.
32. Gentekos DT, Dupuis LN, Fors BP (2016) Beyond dispersity: Deterministic control of polymer molecular weight distribution. *J Am Chem Soc* 138:1848–1851.
33. Pastre JC, Browne DL, Ley SV (2013) Flow chemistry syntheses of natural products. *Chem Soc Rev* 42:8849–8869.
34. Adamo A, et al. (2016) On-demand continuous-flow production of pharmaceuticals in a compact, reconfigurable system. *Science* 352:61–67.
35. Leibfarth FA, Johnson JA, Jamison TF (2015) Scalable synthesis of sequence-defined, unimolecular macromolecules by Flow-IEG. *Proc Natl Acad Sci USA* 112:10617–10622.
36. Jewett JC, Bertozzi CR (2010) Cu-free click cycloaddition reactions in chemical biology. *Chem Soc Rev* 39:1272–1279.
37. Jewett JC, Sletten EM, Bertozzi CR (2010) Rapid Cu-free click chemistry with readily synthesized biarylazacyclooctynones. *J Am Chem Soc* 132:3688–3690.
38. DeForest CA, Polizzotti BD, Anseth KS (2009) Sequential click reactions for synthesizing and patterning three-dimensional cell microenvironments. *Nat Mater* 8:659–664.
39. Johnson JA, Baskin JM, Bertozzi CR, Koberstein JT, Turro NJ (2008) Copper-free click chemistry for the in situ crosslinking of photodegradable star polymers. *Chem Commun (Camb)* (26):3064–3066.
40. Zhao H, Sterner ES, Coughlin EB, Theato P (2012) o-Nitrobenzyl alcohol derivatives: Opportunities in polymer and materials science. *Macromolecules* 45:1723–1736.
41. Johnson JA, Finn MG, Koberstein JT, Turro NJ (2007) Synthesis of photocleavable linear macromonomers by ATRP and star macromonomers by a tandem ATRP–click reaction: Precursors to photodegradable model networks. *Macromolecules* 40:3589–3598.
42. Gordon CG, et al. (2012) Reactivity of biarylazacyclooctynones in copper-free click chemistry. *J Am Chem Soc* 134:9199–9208.
43. Hammouda B, Ho DL, Kline S (2004) Insight into clustering in poly(ethylene oxide) solutions. *Macromolecules* 37:6932–6937.
44. Nishi K, et al. (2014) Small-angle neutron scattering study on defect-controlled polymer networks. *Macromolecules* 47:1801–1809.
45. Hayashi K, et al. (2017) Fast-forming hydrogel with ultralow polymeric content as an artificial vitreous body. *Nat Biomed Eng* 1:0044.
46. Lin-Gibson S, Jones RL, Washburn NR, Horkay F (2005) Structure-property relationships of photopolymerizable poly(ethylene glycol) dimethacrylate hydrogels. *Macromolecules* 38:2897–2902.
47. Waters DJ, et al. (2010) Morphology of photopolymerized end-linked poly(ethylene glycol) hydrogels by small angle X-ray scattering. *Macromolecules* 43:6861–6870.
48. Wang R, Alexander-Katz A, Johnson JA, Olsen BD (2016) Universal cyclic topology in polymer networks. *Phys Rev Lett* 116:188302.
49. Wang R, Johnson JA, Olsen BD (2017) Odd–even effect of junction functionality on the topology and elasticity of polymer networks. *Macromolecules*, 10.1021/acs.macromol.6b01912.
50. Sakai T, et al. (2008) Design and fabrication of a high-strength hydrogel with ideally homogeneous network structure from tetrahedron-like macromonomers. *Macromolecules* 41:5379–5384.
51. Akagi Y, Matsunaga T, Shibayama M, Chung U-i, Sakai T (2010) Evaluation of topological defects in tetra-PEG gels. *Macromolecules* 43:488–493.